

Optical and Raman spectroscopy studies on Fe-based superconductors

W. Z. Hu^a, Q. M. Zhang^{b,c}, N. L. Wang^a

^aBeijing National Laboratory for Condensed Matter Physics, Institute of Physics, Chinese Academy of Sciences, Beijing 100190, P. R. China

^bDepartment of Physics, Renmin University of China, Beijing 100872, P. R. China

^cNational Laboratory of Solid State Microstructures, Department of Physics, Nanjing University, Nanjing 210093, P. R. China

Abstract

A brief review of optical and Raman studies on the Fe-based superconductors is given, with special emphasis on the competing phenomenon in this system. Optical investigations on ReFeAsO (Re=rare-earth element) and AFe_2As_2 (A=alkaline-earth metal) families provide clear evidence for the gap formation in the broken symmetry states, including the partial gaps in the spin-density wave states of parent compounds, and the pairing gaps in the superconducting states for doped compounds. Especially, the superconducting gap has an s-wave pairing lineshape in hole-doped BaFe_2As_2 . Optical phonons at zone center detected by Raman and infrared techniques are classified for several Fe-based compounds. Related issues, such as the electron-phonon coupling and the effect of spin-density wave and superconducting transitions on phonons, are also discussed. Meanwhile, open questions including the T -dependent mid-infrared peak at 0.6-0.7 eV, electronic correlation, and the similarities/differences between high- T_c cuprates and Fe-based superconductors are also briefly discussed. Important results from other experimental probes are compared with optical data to better understand the spin-density wave properties, the superconductivity, and the multi-band character in Fe-based compounds.

Key words: spin-density waves, superconductivity, iron pnictides, infrared and Raman spectroscopy

PACS: 78.20.-e, 78.30.-j, 75.30.Fv, 74.25.Gz, 74.25.Kc

1. Introduction

A new family of high temperature superconductors containing FeAs layers has attracted a broad interest since the discovery of superconductivity in $\text{LaFeAsO}_{1-x}\text{F}_x$ ($x=0.05\sim 0.12$) with $T_c=26$ K by Kamihara *et al.*[1] When replacing the La ion by other rare-earth elements (Ce, Nd, Pr, Sm), T_c could be raised to 40~55 K.[2, 3, 4] In analogy with the high- T_c cuprates, those quaternary oxypnictides adopt a layered structure with the Fe_2As_2 tetrahedron as an essential structural unit, in which the superconductivity appears when the antiferromagnetic ordering for this Fe-layer is suppressed by doping. However, unlike the cuprates where the undoped parent compounds are antiferromagnetic Mott insulators, the ReFeAsO (Re=La, Ce, Nd, Pr, Sm, etc.) parent compounds are metals or semimetals. The magnetic phase for the Fe-based parent compounds is identified as a spin-density wave (SDW) ordering.[5, 6]

Although the first FeAs superconductors are found on doped variants of ReFeAsO , it is soon reported that superconductivity could be induced in other types of structure containing the same tetrahedrally coordinated Fe_2As_2 (or Fe_2Se_2) layers as in ReFeAsO compounds. Those include the oxygen-free AFe_2As_2 (A=Ca, Sr, Ba, Eu) (122-type) [7, 8, 9, 10, 11, 12, 13, 14, 15, 16], $\text{FeSe}(\text{Te})$ (11-type) [17, 18] and Li_xFeAs (111-type) [19, 20, 21]. Up to now, many of research works have been done on 122-type materials. This is because high-quality single

crystals with sufficient sizes for different measurements could be easily grown for this type of Fe-based compounds, although their maximum T_c does not exceed 38 K.

Optical and Raman spectroscopies are powerful experimental techniques in determining the charge dynamics and phonon response for solids. In this article, we briefly summarize current progress in optical and Raman spectroscopic studies, including the normal state properties, the SDW partial gap and superconducting gap, electronic correlation, and phonon spectra for Fe-based compounds. Comprehensive overviews on various physical properties for the superconducting Fe-based compounds could be found in this special issue on pnictide superconductors or in a recent review article by Sadovskii. [22]

In the early stage, infrared spectroscopic studies on polycrystalline Fe-based compounds provide primitive information for the energy gaps in the broken symmetry states. The SDW partial gap is evidenced as a spectral suppression in the far-infrared for LaFeAsO , with a metallic response near the low frequency limit.[5, 3] Optical signature of the superconducting gap is also observed in superconducting $\text{ReFeAsO}_{1-x}\text{F}_x$ polycrystals[23, 24]. When high-quality single crystalline AFe_2As_2 becomes available, convinced spectroscopic evidence are obtained for the in-plane charge dynamics. Direct observation of the SDW partial gap in AFe_2As_2 , and the s-wave symmetry of superconducting gap in $\text{Ba}_{0.6}\text{K}_{0.4}\text{Fe}_2\text{As}_2$ are reported.[25, 26] Optical evidence for the s-wave superconducting gap indicates that the newly discovered Fe-based superconductor is apparently distinguishable from the high- T_c cuprates.

Email address: nlwang@aphy.iphy.ac.cn Tel: +86-10-8264 9584. (N. L. Wang)

More interestingly, both the SDW gap in parent compounds and the superconducting gap in the doped superconductors show a double-gap character for AFe_2As_2 -type compound, reflecting the multi-band property in Fe-based system. Spectroscopic studies on single crystalline 122- and 1111-type Fe-based superconductors suggest the electronic correlation is moderate, with a possible electron-boson coupling signature in the optical quasiparticle self-energy, but the scattering rate $1/\tau(\omega)$ shows apparently different response to that of high- T_c cuprates. A 0.6-0.7 eV mid-infrared feature is observed for both ReFeAsO and AFe_2As_2 systems, with a spectral weight redistribution to higher energies as decreasing T . Whether this high energy feature is a pseudogap or just an interband transition remains an open question.

The resistivity and free-carrier concentration of iron-based superconductors and their parent compounds are comparable to those of cuprates, which can be estimated by the published transport, Hall and infrared measurements and first-principle calculations. However, both experiments and theoretical calculations indicate that the Fe-based compounds show multi-band structures of d -orbitals, which can effectively increase the itinerancy of electrons and decrease electronic correlation. Consequently this would lead to a relatively enhanced Coulomb screening, which may raise the difficulties in searching for electronic Raman scattering signals. As we know, electronic Raman scattering detects density-density correlation in the charge channel. So far, studies on the zone center optical phonons obtain consistent results, while the ratio of signal to noise is low in Raman measurements compared to the case of cuprates. Raman and infrared active modes are investigated in combination with first-principle calculations. Compatible results are obtained by different groups. Raman, inelastic X-ray scattering measurements, and isotope effect experiments etc. provide important clues on the electron-phonon coupling in the Fe-based materials. Considering the similarities between the antiferromagnetic state in cuprates and the SDW state in the parent compounds of iron-based superconductors, it will be very interesting to explore if some magnetic excitations similar to two-magnon process can be observed by inelastic light scattering. Unfortunately, no such magnetic Raman scattering is reported at present.

2. Spin-density wave in the parent compound

An important progress in understanding the FeAs-based compounds is the identification of the SDW order in the parent compound. As we shall explain, essential information was obtained from the infrared spectroscopy measurement.

2.1. SDW in ReFeAsO

The FeAs-based system shows an interesting competing phenomenon. As shown in Fig. 1, the undoped LaFeAsO compound itself is not superconducting, but shows a strong anomaly near 150 K, below which the resistivity drops steeply. With fluorine doping, the anomaly shifts to lower temperature, and gradually disappears, then superconducting transition occurs.

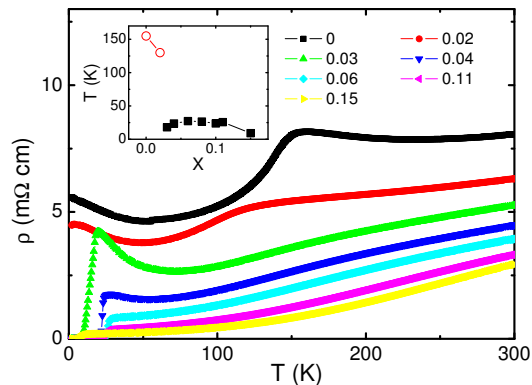


Figure 1: The temperature dependent resistivity for a series of $\text{LaFeAsO}_{1-x}\text{F}_x$ polycrystals. Inset: The phase diagram showing the anomaly (red circle) and superconducting transition (black square) temperatures as a function of fluorine content. [5]

Apparently, superconductivity competes with the phase showing the anomaly in this system. The anomaly was already observed in the earliest report by Kamihara *et al.*[1], however its origin was not addressed there. The first work of identifying the nature of this anomaly was done by Dong *et al.* in a combined experimental studies of transport/optical properties and first-principle band structure calculations.[5] Dong *et al.* found a very clear specific heat jump from specific heat measurement, suggesting that the anomaly is a second-order phase transition. Furthermore, the electronic specific heat coefficient determined at low temperature, $\gamma=3.7$ mJ/mol K^2 , is significantly smaller than the value obtained from the band structure calculations (about 5.5-6.5 mJ/mol K^2). Such a discrepancy is unconventional, because the band structure calculation usually gives a smaller value than the experimental data, and their difference is ascribed to the renormalization effect. Here a natural explanation for a larger theoretically predicted value is that a partial energy gap opens, which removes parts of the density of states below the phase transition temperature. This is indeed seen in their optical spectroscopy experiments on the parent compound.

Figure 2 shows the far-infrared reflectivity $R(\omega)$ and conductivity $\sigma_1(\omega)$ for polycrystalline LaFeAsO . [5] Regardless of the five phonon modes in the far-infrared, one can find the reflectance is strongly suppressed below 600 cm^{-1} at low temperature. This leads to a loss of low-frequency spectral weight in the real part of conductivity $\sigma_1(\omega)$ as shown in Fig. 2b. In fact, the $\sigma_1(\omega)$ already shows a weak suppression at 140 K, which becomes more apparent as decreasing temperature. A spectral suppression in the free-carrier contribution indicates a reduction of itinerant carriers, thus is an optical evidence for the energy gap on the Fermi surface. As the reflectance at very low frequency increases fast and exceeds the values at high temperature, the compound is still metallic even below the phase transition, being consistent with the enhanced dc conductivity. The data indicate clearly that the Fermi surfaces are only partially gapped.

Identification of a gap formation below the phase transition strongly suggests that the anomaly is caused by a symmetry-

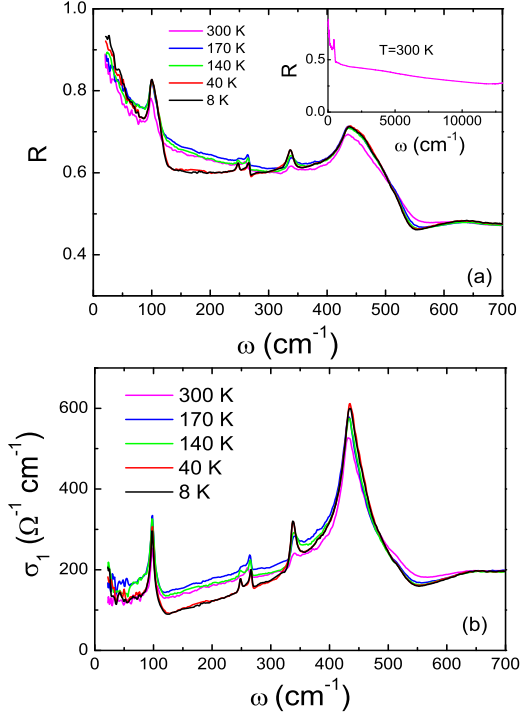


Figure 2: The optical reflectivity $R(\omega)$ and the real part of conductivity for LaFeAsO polycrystal.[5]

breaking phase transition, i.e. either a charge-density wave (CDW) or an SDW instability. In the far-infrared spectra, one can see several infrared-active phonon modes roughly at 100, 247, 265, 336, 438 cm^{-1} , but no splitting or new phonon modes develop below the transition. This indicates that the structural distortion associated with the transition, if any, should be rather small. On this basis, Dong *et al.* suggest that the phase transition is unlikely to be driven by a CDW instability but an SDW instability. Further convincing evidence for an SDW instability comes from the first-principle band structure calculations presented in the same work,[5] where the authors find a strong nesting effect between the hole Fermi surface surrounding the zone center and the electron Fermi surface centered at the zone corner.

The Fermi surface nesting in LaFeAsO has a commensurate wave vector $\mathbf{q}=(\pi, \pi)$, leading to a doubling of the unit cell of $\sqrt{2} \times \sqrt{2}$ along diagonal directions. Suppose that an antiferromagnetic ordering is associated with the lattice structure, a stripe- or collinear-type antiferromagnetic pattern would develop below the phase transition temperature with such a (π, π) nesting vector.[5] Further calculation indicates that the LaFeAsO parent compound would have a lower total energy in such antiferromagnetic ordered phase with respect to the nonmagnetic phase. Furthermore, the density of state at the Fermi level is reduced significantly compared with the original nonmagnetic phase, in accordance with a small specific heat value from transport measurement, and a gap from optical spectroscopy. Therefore, the SDW order for the parent compound is identified convincingly.

Conclusive evidence for the spin-density wave order is obtained from neutron experiments. Clarina de la Cruz *et al.*[6] performed neutron diffraction measurement on LaFeAsO and demonstrated that an antiferromagnetic ordering develops at low temperature. In particular, the spin structure determined by their neutron experiment is identical to the spin configuration predicted based on the nesting of hole and electron Fermi surfaces proposed by Dong *et al.*[5] However, the neutron experiments also revealed a very subtle structural distortion near 150 K, which accounts for the resistivity anomaly, while a magnetic ordering develops at a slightly lower temperature for LaFeAsO polycrystal. It is now widely believed that the structural distortion is driven by the magnetic instability.[27, 28, 29, 30]

Optical reflectance investigations were also carried out on other 1111-type polycrystalline parent compounds.[3, 31, 32] Shortly after the work on LaFeAsO $_{1-x}$ F $_x$, Chen *et al.*[3] used the rare-earth element Ce to replace La and synthesize a series of CeFeAsO $_{1-x}$ F $_x$ compounds. Interestingly, in this rare-earth based 1111 compound, a much higher T_c (41 K) is achieved. From transport and optical spectroscopy measurement they identified very similar competing phenomenon between spin-density wave and superconductivity in CeFeAsO $_{1-x}$ F $_x$. Neutron experiment also revealed a stripe type antiferromagnetic order of the Fe sublattice in the parent compound, being identical to the LaFeAsO compound.[33] The similarity between La- and Ce-based compounds suggest that the interplay between the superconductivity and the spin-density wave instability is a common phenomenon for FeAs-based systems. Additionally Chen *et al.* found that the Ce 4f electrons form local moments and ordered antiferromagnetically below 4 K, which coexists with superconductivity in CeFeAsO $_{1-x}$ F $_x$.

The optical suppression (i.e., the SDW gap) is found for different types of ReFeAsO samples, however, as the optical data are collected on polycrystals, the $R(\omega)$ is dominated by several strong phonon modes related to the weakly conducting c-axis response.[31] In particular, a strong oxygen-derived phonon mode[34, 35] around 438 cm^{-1} weakens the ab-plane charge dynamics, it is therefore difficult to accurately define the energy scale affected by the SDW gap. Boris *et al.*[36] report an infrared ellipsometry study on polycrystalline LaFeAsO parent compound and 10% F-doped superconductor LaFeAsO $_{1-x}$ F $_x$, and found that the SDW-induced suppression in the optical conductivity $\sigma_1(\omega)$ has a rather large energy scale. Figure 3 shows the optical conductivity for both the parent and the F-doped samples. There is a low energy feature around 0.16 eV in LaFeAsO (ω_{PG}^* in Fig. 3b), and the $\sigma_1(\omega)$ for 10 K is suppressed below that of 300 K for $\omega < \omega_{PG}^*$. This 0.16 eV feature disappears in the superconducting compound (Fig. 3c). As F-doping suppress the antiferromagnetic transition, the 0.16 eV feature in LaFeAsO should be the SDW gap for the parent compound. Our published data on LaFeAsO[5] only show the spectra below 700 cm^{-1} (see Fig. 2), it is not clear whether the energy scope for the SDW-gap induced suppression extends to higher energies. In our latter study on another LaFeAsO polycrystal with higher quality (Fig. 4), the optical suppression indeed extend towards high frequency region, in agreement with the energy scale of 0.16 eV observed by Boris *et al.*

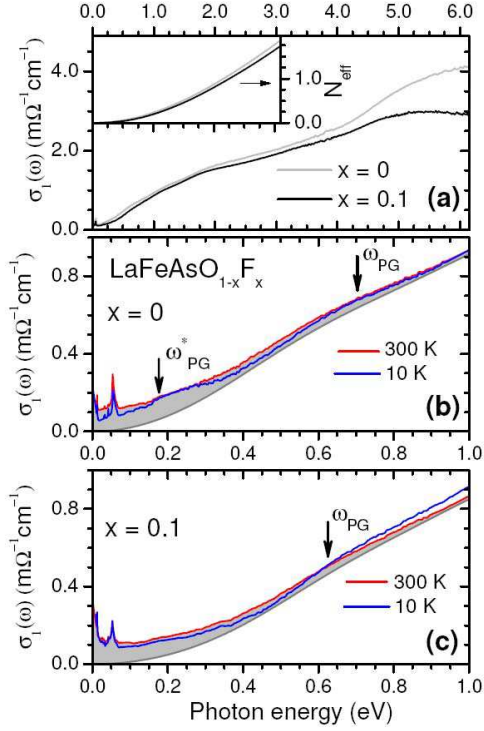


Figure 3: (a) The optical conductivity $\sigma_1(\omega)$ for LaFeAsO (gray) and LaFeAsO_{0.9}F_{0.1} (black) at T=300 K. The $\sigma_1(\omega)$ below 1 eV for (b) LaFeAsO_{0.9}F_{0.1} and (c) LaFeAsO at 10 K and 300 K. The dark gray lines is the low-energy tail of the interband transitions. The shaded area is the contribution from intraband response. The pseudogap is marked by arrows.[36]

Boris *et al.* report another gap-like feature around 0.65 eV for both LaFeAsO and F-doped samples (see Fig. 3b and c), which is suggested to be a pseudogap.[36] Meanwhile, there is a significant spectral weight transfer for the parent and F-doped compounds. In LaFeAsO, the spectral weight redistribution associated with the pseudogap at 0.65 eV is restricted below 2 eV; while for superconducting LaFeAsO_{0.9}F_{0.1}, a substantial spectral weight transfer from below 2 eV to above 4 eV with increasing temperature is observed.[36]

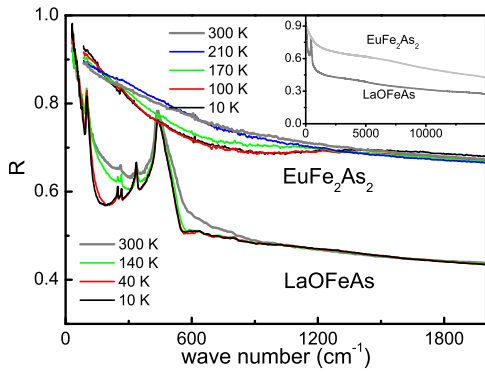


Figure 4: The optical reflectivity $R(\omega)$ for EuFe₂As₂ and LaOFeAs polycrystals.[37]

2.2. SDW in AFe₂As₂

After numerous attempts in Re-site chemical substitution for ReFeAsO, the maximum T_c for this 1111-family is still below 56 K. Therefore, finding new structures containing the FeAs layer becomes the central task in materials research. ThCr₂Si₂-type compound AFe₂As₂ (A=Ba, Sr, Eu) is one of the important findings in the exploration for new types of Fe-based compound.[7] Figure 4 compares the optical reflectivity for polycrystalline LaFeAsO and EuFe₂As₂ ($T_{SDW}=190$ K).[37] One can find the spectral suppression related to SDW partial gap has a larger energy scale for EuFe₂As₂ than LaFeAsO. This could be due to the higher SDW transition temperature for EuFe₂As₂. In addition, the overall $R(\omega)$ for EuFe₂As₂ is substantially higher than that of LaFeAsO, suggesting a larger optical conductivity for EuFe₂As₂. Furthermore, only one weak phonon mode around 262 cm⁻¹ is seen in EuFe₂As₂, indicating screening from the conducting carriers is much better in the 122 system.

The discovery of superconductivity in hole doped ternary iron arsenide (Ba,K)Fe₂As₂[8] immediately attracts considerable interest in this 122 system.[9, 10, 11, 12, 13, 14] Benefited from high-quality single crystals, optical studies on the 122-type compounds achieve more profound progress than that in the 1111 system. A detailed optical study on single crystal samples of BaFe₂As₂ and SrFe₂As₂ parent compounds was reported by Hu *et al.*[25]. In this report, a double-gap character was found for both compounds, along with a dramatic reduction for the free-carrier spectral weight and scattering rate below T_{SDW} .

2.2.1. SDW double-gap

Figure 5 demonstrates the low frequency optical conductivity for BaFe₂As₂ ($T_{SDW}=138$ K) and SrFe₂As₂ ($T_{SDW}=200$ K). The Drude-like conductivity is seen at high temperature. However, a severe suppression of the Drude component is seen at low temperature, and the lost spectral weight gradually piles up into the absorption peaks at higher energies, suggesting a large amount of density of states are removed from E_F by the energy gap for $T < T_{SDW}$. Interestingly, a double-peak structure is seen in the conductivity spectra. Considering the multi-band property for AFe₂As₂,[38] the double peaks in $\sigma_1(\omega)$ should correspond to two SDW gaps on separated Fermi surfaces. Here we note the absorption peaks in $\sigma_1(\omega)$ develop just below T_{SDW} , and the gap-like peaks no longer exist in the nonmagnetic state. Even for 205 K, which is just 5 K above the T_{SDW} in SrFe₂As₂, no gap signature can be found. Therefore, the fluctuation effect for the SDW should be rather weak in AFe₂As₂. From the gap values and SDW transition temperatures, we obtained the ratio of $2\Delta/k_B T_{SDW} \approx 3.5-3.6$ for the smaller gap, and 9-9.6 for the larger gap for the two compounds. The smaller gap coincides roughly with the gap value expected by the conventional BCS relation, while the large one is very different.

Because of the presence of two different gap values in the SDW ordered state, direct information on where the FS sheets are gapped is highly desired. Several angle resolved photoemission spectroscopy (ARPES) investigations on AFe₂As₂ (A=Ba

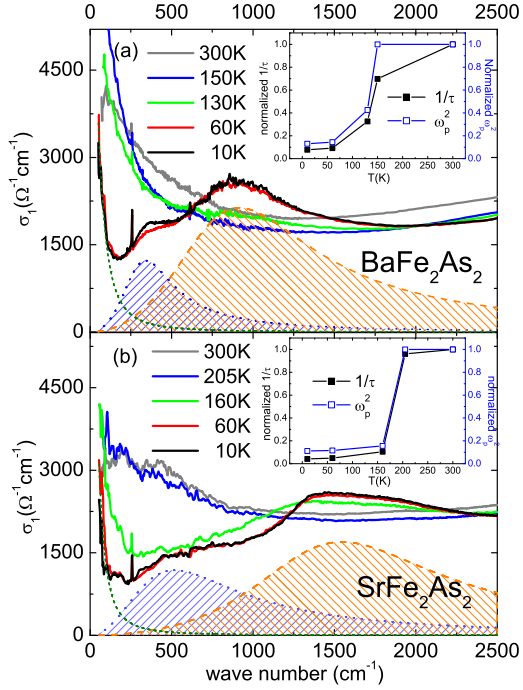


Figure 5: The real part of conductivity $\sigma_1(\omega)$ for (a) BaFe_2As_2 and (b) SrFe_2As_2 below 2500 cm^{-1} . The Drude term (short dash green line) and the first two Lorentz peaks abstracted from a Drude-Lorentz fit for $T=10$ K is shown at the bottom. Inset: normalized $1/\tau$ (black) and ω_p^2 (blue).[25]

or Sr) single crystals have been reported, however, two earlier works by Yang *et al.*[39] and Liu *et al.*[40] reported complete absence of SDW gaps, in sharp contrast to the infrared spectroscopy result. Very recently, Hsieh *et al.* report an orbital resolved ARPES study on SrFe_2As_2 , and find evidence for an anisotropic SDW gap with energy scales on the order of 50 meV, which thus tends to be consistent with optical results.[41]

2.2.2. Free-carrier response

It is well-known that the low- ω Drude component comes from the itinerant carrier contribution. The Drude spectral weight determines the ω_p^2 (ω_p is the plasma frequency), which is proportional to n/m_{eff} (where n is the carrier density, m_{eff} is the effective mass); while its width reflects the carrier scattering rate $1/\tau$. As shown in Fig. 5, Drude components are present not only at $T > T_{SDW}$, but also in the SDW state below the gap-induced absorption peaks. Therefore, the Fermi surface of AFe_2As_2 is only partially gapped below T_{SDW} . Using a Drude-Lorentz fit,[42] we can extract the free-carrier contribution from $\sigma_1(\omega)$. The room T plasma frequency is 12900 cm^{-1} for BaFe_2As_2 , and 13840 cm^{-1} for SrFe_2As_2 . Although the plasma frequency is larger than 1.5 eV, one should also note the scattering rate for the normal state is rather large, i.e., 700 cm^{-1} for BaFe_2As_2 and 950 cm^{-1} for SrFe_2As_2 . Such a large scattering rate corresponds to an overdamped plasma edge in $R(\omega)$. [25] Below the SDW transition, both the plasma frequency and the scattering rate are dramatically reduced. The variations of $1/\tau$ and ω_p^2 with temperature for the Drude term are shown in the insets of Fig. 5. Both parameters are normalized to

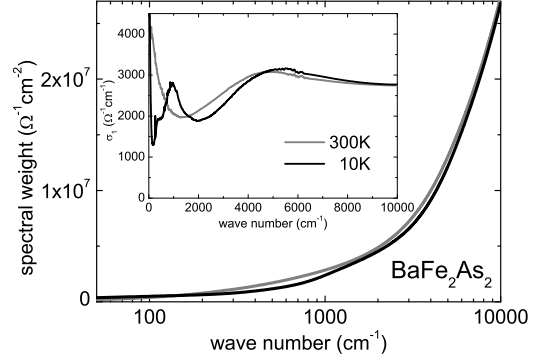


Figure 6: The spectral weight for BaFe_2As_2 below 10000 cm^{-1} . Inset: $\sigma_1(\omega)$ below 10000 cm^{-1} (together with the low- ω extrapolation based on the dc conductivity).[25]

their 300 K value. Provided the effective mass of itinerant carriers does not change with temperature, then the residual carrier density is only 12% of that at high temperature for both compounds. This means that roughly 88% of FS is removed by the gapping associated with SDW transitions. On the other hand, the scattering rate was reduced by about 92-96%. Therefore, the opening of the SDW partial gap strongly reduces the scattering channel, leading to a metallic behavior with enhanced dc conductivity in the gapped state. In the quantum oscillation measurement on SrFe_2As_2 single crystal, a large reduction of the paramagnetic Fermi surface by SDW transition is also observed, then the remaining Fermi surface pockets are only 2% of the original Brillouin zone area in the low T phase.[43]

It should be remarked that the driving mechanism for the SDW instability in the parent compound is currently under debate. Although the stripe- or collinear-type antiferromagnetic order in the SDW state was first suggested to result from the nesting between the hole and electron Fermi surfaces (FS) of itinerant electrons,[5] it was alternatively proposed that the superexchange interaction of Fe ions mediated through the off-plane As atom plays a key role in the spin configuration formation.[27, 28, 29, 30, 44, 45] A stripe-type AFM would arise when the superexchange interaction between next-nearest-neighbor Fe sites becomes larger than half of the nearest-neighbor exchange interaction. The optical study of Hu *et al.* shed light on this debating issue. Their data clearly demonstrate that the parent compounds are metallic both above and below SDW ordering temperatures. They have relatively high plasma frequency (a bit higher than 1.5 eV) in the normal phase. Furthermore, the partial gap values below SDW ordering temperatures are consistent with the expectation of nesting scenario where the temperature dependence of the gap should resemble that of BCS theory. Therefore, Hu's work further favors the itinerant picture for the SDW instability.[5] Under such an itinerant picture, superconductivity in the doped system is mediated by spin fluctuation,[46, 47] where a sign reversal of the order parameters between different Fermi surfaces is obtained.

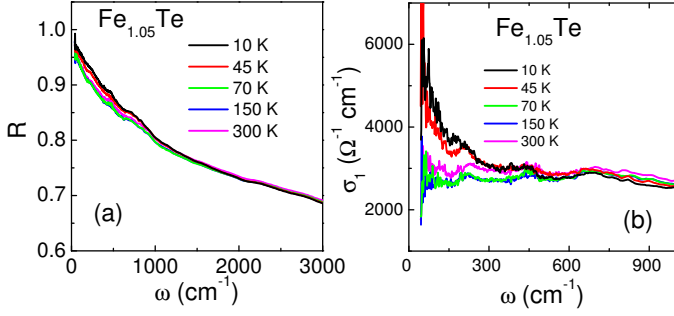


Figure 7: (a) Reflectivity $R(\omega)$ and the real part of conductivity $\sigma_1(\omega)$ for $\text{Fe}_{1.05}\text{Te}$. [59]

2.2.3. High energy feature

As mentioned above, Boris *et al.* observe a high energy pseudogap around 0.65 eV for LaFeAsO and $\text{LaFeAsO}_{0.9}\text{F}_{0.1}$ (Fig. 3), here similar T -dependent feature around 5000 cm^{-1} (0.62 eV) also exists in BaFe_2As_2 and SrFe_2As_2 . Figure 6 is the spectral weight analysis for BaFe_2As_2 , from which two characteristic energy scales can be found: the first one below 2000 cm^{-1} and the second one above 2000 cm^{-1} up to 10000 cm^{-1} . In the first range ($\omega \leq 2000 \text{ cm}^{-1}$), the narrowing of the Drude peak and the development of the SDW double-gap in the mid-infrared lead to a spectral weight redistribution from the free-carrier contribution into the gap induced absorption peaks as decreasing T (see the conductivity data in Fig. 5a for comparison). This redistribution process is not complete until 2000 cm^{-1} , which is an energy scale related with the SDW gap. In the second range ($2000\text{-}10000 \text{ cm}^{-1}$), there is another T -dependent spectral weight transfer from low to high energies due to the 5000 cm^{-1} peak in $\sigma_1(\omega)$. This feature does not directly related with T_{SDW} as it exists even in the non-magnetic state. [25] As shown in the inset of Fig. 6, the 5000 cm^{-1} mid-infrared peak dominates the conductivity spectrum for 300 K, which slightly moves towards higher energies for $T=10 \text{ K}$. Correspondingly, the low frequency spectral weight also shifts towards higher frequencies at low T , and the total spectral weight recovers to normal-state value near 9000 cm^{-1} (Fig. 6).

Similar mid-infrared component has been observed in the doped sample, e.g., $(\text{Ba},\text{K})\text{Fe}_2\text{As}_2$ [26] and $\text{Ba}(\text{Fe},\text{Co})_2\text{As}_2$, and the temperature evolution for this 5000 cm^{-1} peak seems unchanged in these doped systems. Such a high energy feature suggests the incoherent part for Fe $3d$ bands. Strictly speaking, one can not tell whether it is an interband transition or a pseudogap based on current optical data. Anyhow, here we note that a strong band renormalization in the 122-type compounds is found from recent ARPES studies. [41, 48, 49, 50, 51, 52] Therefore, the energy scales for possible interband transitions calculated from the LDA (local-density approximation) might deviate from experimental observation. The origin of this mid-infrared feature requires further studies.

2.3. Absence of the SDW gap for Fe_{1+y}Te

As shown above, the SDW gap induced suppression can be found for both ReFeAsO and AFe_2As_2 . However, the 11-type

single crystalline $\text{Fe}_{1.05}\text{Te}$, which undergoes a structural distortion along with the establishment of a long range antiferromagnetic order near 65K, [53, 54] shows no clear signature of the SDW gap.

Superconductivity with transition temperature T_c up to 15 K was obtained on $\text{Fe}_{1+x}(\text{Se},\text{Te})$ system at ambient pressure. [55, 56, 57] The T_c can go up to 27 K at a pressure of 1.48 GPa. [58] Figure 7 shows the reflectivity $R(\omega)$ and the real part of conductivity $\sigma_1(\omega)$ for $\text{Fe}_{1.05}\text{Te}$. [59] The normal state reflectivity is similar to AFe_2As_2 , [25] that $R(\omega)$ has an almost linear frequency dependence up to mid-infrared region. It is important to note that the conductivity spectra above T_{SDW} are rather flat. Definitely, it is not a semiconductor as no semiconductor-like gap could be found in $\sigma_1(\omega)$, but it is not a simple metal as well, because of the absence of a Drude-like peak. As is well known, the width of Drude peak is determined by the scattering rate (or inverse of the transport lifetime) of the quasiparticle, the measurement result indicates that there is no well defined quasiparticle with sufficiently long transport life time above T_{SDW} . The charge transport is rather incoherent. Below T_{SDW} , the low- ω $R(\omega)$ increases fast. Correspondingly, a Drude component in $\sigma_1(\omega)$ develops quickly from the incoherent background. Unlike the parent compounds of LaFeAsO and AFe_2As_2 ($A=\text{Ba}, \text{Sr}$), there is no partial gap formation in optical spectra below T_{SDW} . [59] The absence of SDW gap formation has been confirmed by recent ARPES experiment on $\text{Fe}_{1.05}\text{Te}$. [60] Those data, together with transport and specific heat measurement results, suggest that $\text{Fe}_{1+x}(\text{Se},\text{Te})$ system is an exceptional case. This was presumably attributed to the presence of excess Fe^{1+} ions, which have large magnetic moments and locate randomly in the Fe(2) sites as in Fe_2As compound, resulting in rather strong interaction with the magnetism of FeTe layers. [61, 59]

3. Superconductivity in the doped compound

Probing the energy scale and the symmetry of the superconducting gap are always important tasks for infrared spectroscopy. In the early stage, when only 1111-type polycrystals are available, the superconducting gap was observed as an abrupt increase of reflectivity in $\text{LaFeAsO}_{1-x}\text{F}_x$. [23] Soon, the superconducting gap in $(\text{Nd},\text{Sm})\text{FeAsO}_{0.82}\text{F}_{0.18}$ polycrystals were found by infrared ellipsometry. [24] In addition, a pronounced dip at 20 meV was found in the reflectivity ratio $R(\omega, T < T_c)/R(\omega, T_n)$ from a series F-doped $\text{SmO}_{1-x}\text{F}_x\text{FeAs}$ polycrystals with unpolished surfaces. [62] The electron-boson coupling was estimated by Drechsler *et al.* based on optical data collected on powder $\text{LaFeAsO}_{0.9}\text{F}_{0.1}$ and reported value of in-plane penetration depth. [63] With the availability of single crystalline samples of $(\text{A},\text{K})\text{Fe}_2\text{As}_2$ ($A=\text{Sr}, \text{Ba}$), more reliable in-plane optical data were obtained. The first optical evidence for an s-wave superconducting gap was found in $\text{Ba}_{0.6}\text{K}_{0.4}\text{Fe}_2\text{As}_2$, [26] where the in-plane $R(\omega)$ suddenly turns up and approaches unity below T_c , following the well-established BCS description.

3.1. Probing the superconducting gap

Three length scales characterize the electrodynamics of superconductors, i.e., the London penetration depth λ_L , the correlation length ξ_0 , and the mean free path of the uncondensed electrons l . The London penetration depth $\lambda_L=c/\omega_{ps}$, where ω_{ps} is the plasma frequency for the condensed carriers. The penetration depth is a characteristic scale within which the external magnetic field is exponentially screened. The correlation length ξ_0 is the spatial extension of the Cooper pairs.[64, 42] For superconductors, the dirty limit is the case in which $l \ll \xi_0$, thus the width of the Drude term $1/\tau$ in the normal state should be larger than the superconducting gap 2Δ ; while the clean limit is a case that $l \gg \xi_0$, thus $1/\tau \ll 2\Delta$. The dirty limit and the clean limit can be distinguished by their different spectral responses across the superconducting transition. In the clean limit, no clear signature of the superconducting gap could be found in $\sigma_1(\omega)$, because the spectral weight for the superconducting condensate lies below 2Δ , so that there is no detectable change of spectrum at the gap energy 2Δ across the T_c . In the dirty limit, the normal-state Drude term is broader than 2Δ , therefore the disappearance of single-particle excitation below 2Δ would left an incoherent contribution in $\sigma_1(\omega)$, and the normalized spectral weight of the superconducting condensate converges much more slowly than in the clean-limit case. [65, 66]

According to the optical sum rule[42] $\int \sigma_1(\omega)d\omega=\omega_p^2/8$, the area under $\sigma_1(\omega)$ should be conserved, and the total spectral weight is determined by the effective carrier density as the plasma frequency $\omega_p^2=4\pi Ne^2/m_{eff}$. In this sense, the lost spectral weight in $\sigma_1(\omega)$ below T_c (so-called "missing area") is a more essential character than the gap in optical spectrum.[64] The "missing area" denotes the existence of superconducting condensate, i.e., a collective excitation at zero frequency with the form of $\delta(\omega)$ function. Using Kramers-Kronig relation, a term $\sigma_1(\omega) = A\delta(\omega)$ corresponds to $\sigma_2(\omega) = 2A/\pi\omega$. Comparing with the London equation $\sigma_2(\omega) = c^2/4\pi\lambda_L^2\omega$, the penetration depth λ calculated from the imaginary part of conductivity should be equal to that calculated from the "missing area" A in the real part of conductivity.[64]

$$\lambda = c/\sqrt{8A} \quad (1)$$

which is the famous Ferrell-Glover-Tinkham (FGT) sum rule.[67, 68] As the imaginary part of the conductivity $\sigma_2(\omega)$ diverges as $1/\omega$ below 2Δ , it can be shown that the optical reflectivity $R(\omega)$ would rapidly approach to unity below the gap energy for BCS superconductor.[42] Therefore, the up-turn in $R(\omega)$ at low frequency for $T < T_c$ is an optical evidence for the superconducting gap, and a rapid saturation of reflectivity indicates the gap is isotropic (s-wave). While for the case of non s-wave pairing, the optical reflectivity will slowly increases towards unity instead of an abrupt jump.

3.2. Superconducting gap in 1111-type polycrystal

The first optical investigation for the superconducting gap in FeAs-based superconductor was done on a $\text{LaFeAsO}_{1-x}\text{F}_x$ polycrystal. Transport measurements testify the existence of superconducting transition, and the ac magnetic susceptibility

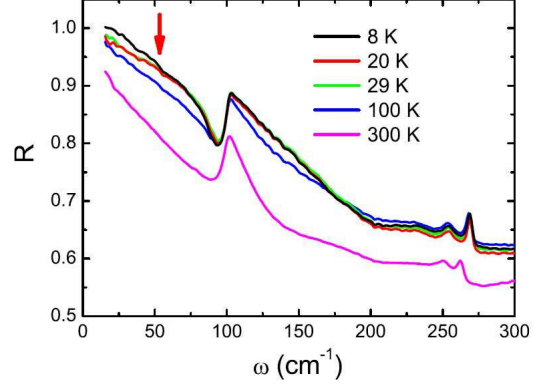


Figure 8: The optical reflectivity $R(\omega)$ for F-doped LaFeAsO polycrystal.[23]

drops at 20 K.[23] Although the spectral change from 29 K to 20 K is hard to resolve in Fig. 8, an evident up-turn for $T=8$ K below $50\sim 60 \text{ cm}^{-1}$ can be found (see the arrow in Fig. 8). Since the up-turn in optical reflectivity $R(\omega)$ corresponds to the onset energy of the superconducting gap, then $2\Delta/kT_c$ is 3.5-4.2 for $\text{LaFeAsO}_{1-x}\text{F}_x$ polycrystal, which is quite close to the prediction by BCS theory. Unlike the conventional BCS-type superconductor, here the reflectivity for $\text{LaFeAsO}_{1-x}\text{F}_x$ does not abruptly approach unity below 2Δ , but gradually increases towards the 100% line. A continuous increase in $R(\omega)$ is a common feature for high- T_c cuprate where the superconducting gap has a d-wave symmetry.[69] However, no conclusion on the gap symmetry could be drawn from optical data on polycrystalline sample.

Further optical evidence for the superconducting gap in Fe-based superconductor is obtained from ellipsometric spectroscopy on polycrystalline $\text{NdFeAsO}_{0.82}\text{F}_{0.18}$ ($T_c=52$ K) and $\text{SmFeAsO}_{0.82}\text{F}_{0.18}$ ($T_c=45$ K).[24] Figure 9a shows the optical conductivity for $\text{NdFeAsO}_{0.82}\text{F}_{0.18}$ polycrystal at selected temperatures. The optical conductivity is dominated by four pronounced phonon modes in the far-infrared region for all temperatures. Regardless of these phonon modes, one can find the T -evolution for $\sigma_1(\omega)$ is changed across T_c : the $\sigma_1(\omega)$ is slightly enhanced due to the metallic response above T_c ; while an obvious gap-like suppression below 300 cm^{-1} could be found for $T < T_c$. The suppression can be more clearly resolved by the "missing area" in $\sigma_1(\omega)$. Figure 9b shows the difference spectrum $\sigma_1(10\text{K})-\sigma_1(55\text{K})$ as a function of frequency, and the inset plots the T -dependent spectral weight between 50 and 300 cm^{-1} . Dubroka *et al.* defines the superconducting gap 2Δ as the onset energy for the optical suppression ω_{SC}^* ($300 \text{ cm}^{-1} \sim 37 \text{ meV}$), thus $2\Delta/k_B T_c \approx 8$.

As shown above, optical signatures of the superconducting gap are found in polycrystalline $\text{LaFeAsO}_{1-x}\text{F}_x$, $\text{SmFeAsO}_{1-x}\text{F}_x$, and $\text{NdFeAsO}_{1-x}\text{F}_x$. However, both methods used in Fig. 8 and 9 to identify the gap onset energy are not accurate. The pronounced phonon mode near 100 cm^{-1} strongly affects the low frequency reflectivity, thus it is difficult to distinguish the exact frequency for the up-turn in $R(\omega)$. While subtracting the normal state spectra to cancel out the phonon information and using ω_{SC}^* (Fig. 9) as the gap will overestimate

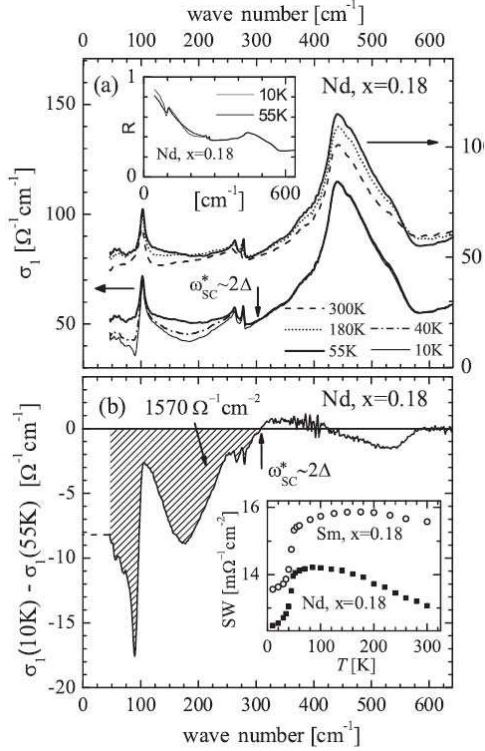


Figure 9: The optical response for NdFeAsO_{0.82}F_{0.18} (Nd, $x=0.18$) and SmFeAsO_{0.82}F_{0.18} (Sm, $x=0.18$) superconductors. (a) $\sigma_1(\omega)$ of the Nd, $x=0.18$ sample. The arrow marks the onset of the superconductivity-induced gaplike suppression. Inset: calculated reflectivity. (b) $\sigma_1(10K) - \sigma_1(55K)$. The shaded area is the missing spectral weight due to the superconducting condensate. Inset: integrated $\sigma_1(\omega)$ (i.e., the spectral weight) between 45 and 300 cm^{-1} . [24]

the gap in the dirty-limit.[65, 66] Then spectroscopic data on the single crystals are highly desirable.

3.3. Superconducting gap in 122-type single crystal

The first optical data on superconducting Ba_{1-x}K_xFe₂As₂ single crystals were reported individually by two groups.[26, 70] Li *et al.* gave evidence for an s-wave superconducting gap in optimally doped Ba_{0.6}K_{0.4}Fe₂As₂, and found the Ferrell-Glover-Tinkham sum rule was satisfied within an energy scale of 6Δ . [26] Yang *et al.* studied the optical properties of Ba_{0.55}K_{0.45}Fe₂As₂ above its superconducting transition temperature (28 K), and concentrated on the normal state properties.[70]

Figure 10 shows the ab-plane optical reflectivity for Ba_{0.6}K_{0.4}Fe₂As₂ ($T_c = 37$ K). The $R(\omega)$ for all $T > T_c$ follow a linear frequency dependence. When $T < T_c$, the $R(\omega)$ suddenly turns up below 300 cm^{-1} and approaches unity around 150 cm^{-1} , which is a typical character for an s-wave superconducting gap.[42] The temperature dependence of the optical conductivity is shown in Fig. 11. The Drude component narrows as decreasing T from 300 K to 45 K. For $T < T_c$, a large amount of the Drude weight in $\sigma_1(\omega)$ collapse into the superconducting condensate at zero frequency, leading to a non-zero excitation above 2Δ , and a "missing area" between 10 K and 45

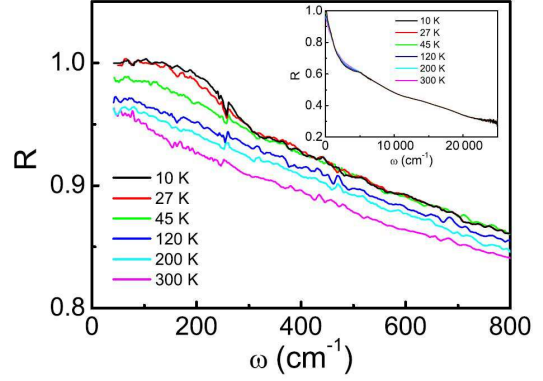


Figure 10: Optical reflectivity $R(\omega)$ for Ba_{0.6}K_{0.4}Fe₂As₂ in the far-infrared region. Inset: The inset shows $R(\omega)$ over a broad frequency range.[26]

K (see the inset figure). As shown in Section 3.1, the "missing area" in $\sigma_1(\omega)$ corresponds to the zero-frequency collective mode. The penetration depth estimated from the missing area is 2080 Å. The same quantity calculated from the imaginary part of optical conductivity $\sigma_2(\omega) = c^2/4\pi\lambda^2\omega$ is $\lambda \approx 1950$ Å. The good agreement for the penetration depth by different calculations indicated the validity of FGT sum rule in Ba_{0.6}K_{0.4}Fe₂As₂. An inspection of the inset of Fig. 11 reveals that the "missing area" extends to the frequency roughly below 600 cm^{-1} , about 3 times larger than the higher superconducting energy gap 2Δ . This indicates that the superconducting condensate forms rapidly or the FGT sum rule is rapidly recovered. This is very different from underdoped high- T_c cuprates where recovery of the FGT sum rule goes to very high energy, or the FGT sum rule is even violated.[65, 71, 72]

According to the BCS theory in the dirty limit, there is no optical excitation for $\hbar\omega < 2\Delta$, while above 2Δ the optical conductivity $\sigma_1(\omega)$ gradually rises due to the case II coherence factor.[64] Since the $\sigma_1(\omega)$ for $\omega < 2\Delta$ is condensed into the zero frequency collective mode, $\sigma_2(\omega)$ will diverge as $1/\omega$ for $\omega < 2\Delta$, then a peak at 2Δ could be found in $R(\omega, T \ll T_c)/R(\omega, T \approx T_c)$. [42] As shown in Fig. 11, the conductivity is almost zero below roughly 150 cm^{-1} due to the flat and

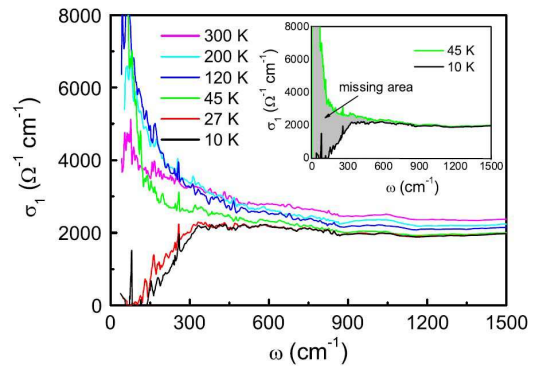


Figure 11: Optical conductivity for Ba_{0.6}K_{0.4}Fe₂As₂. The inset shows $\sigma_1(\omega)$ at 10 and 45 K. The shaded area represents the "missing area" due to the opening of superconducting energy gap.[26]

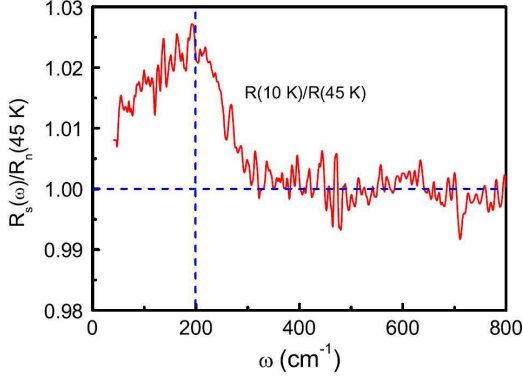


Figure 12: The reflectance ratio $R(\omega, T=10\text{ K})/R(\omega, T=45\text{ K})$. A peak near 200 cm^{-1} is seen.[26]

close to unity $R(\omega)$, which is an optical evidence for the s-wave superconducting energy gap. However, the peak in $R(\omega, 10\text{ K})/R(\omega, 45\text{ K})$ is around 200 cm^{-1} , thus yields a different energy scale for the superconducting gap. According to recent ARPES study on $\text{Ba}_{0.6}\text{K}_{0.4}\text{Fe}_2\text{As}_2$ (where the single crystalline sample comes from the same batch as the one used in optical study[26]), two isotropic gaps ($\Delta_1=6\sim 8\text{ meV}$, $\Delta_2=10\sim 12\text{ meV}$) are found on different Fermi surfaces.[73, 74, 75] Thus the discrepancy in the gap energies from $\sigma_1(\omega)$ and R_s/R_n might also suggest a two-gap character for $\text{Ba}_{0.6}\text{K}_{0.4}\text{Fe}_2\text{As}_2$.

3.4. Coherence factor and the double-gap in $\text{Ba}_{0.6}\text{K}_{0.4}\text{Fe}_2\text{As}_2$

Single electron transitions, induced by external perturbations such as electromagnetic radiation, ultrasound, or nuclear relaxation are determined by coherence factors, in addition to density of state effects.[76] Considering the transition rate α_s between energy levels E and $E'=E+\hbar\omega$,

$$\alpha_s = \int |M|^2 F(\Delta, E, E') N_s(E) N_s(E') [f(E) - f(E')] dE \quad (2)$$

where M is the magnitude of the one-electron matrix element thus $|M|^2$ the transition probability, Δ the single particle gap, $N(E)$ the density of states, $f(E)$ the Fermi distribution function $1/(1+e^{E/k_B T})$, and $F(\Delta, E, E')$ the coherence factor. As shown by Tinkham[64] and Grüner[76], the electromagnetic absorption process for the density-wave and BCS superconducting ground states have different coherence factors since they are invariant under different symmetry operations. Thus,

$$\frac{\sigma_1^S}{\sigma_1^N} = \frac{1}{\hbar\omega} \int_{-\infty}^{\infty} \frac{|E(E+\hbar\omega) \mp \Delta^2| [f(E) - f(E+\hbar\omega)]}{(E^2 - \Delta^2)^{1/2} [(E+\hbar\omega)^2 - \Delta^2]^{1/2}} dE \quad (3)$$

where σ_1^S is the conductivity for the density-wave or superconducting state, σ_1^N the conductivity for the normal state, and the upper sign corresponds to case I (e.g., SDW) and the lower to case II (e.g., BCS superconductor). Calculation for the conductivity ratio based on Eq. 3 requires numerical integration. However, the integral has a simple expression in terms of complete elliptic integrals for $T=0\text{ K}$. [64] The inset of Fig. 13 shows the calculation result based on Eq. 3 for the single-gap case. For the SDW ground state with an isotropic gap

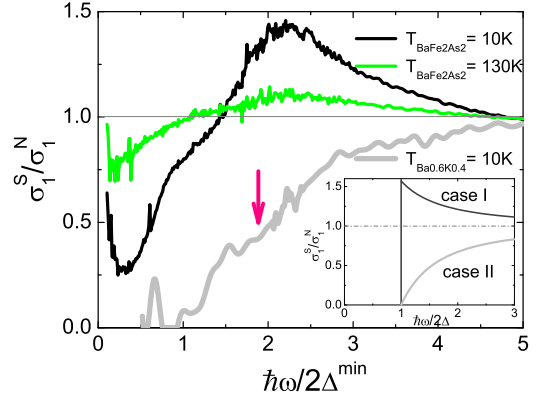


Figure 13: σ_1^S/σ_1^N for BaFe_2As_2 and $\text{Ba}_{0.6}\text{K}_{0.4}\text{Fe}_2\text{As}_2$. The double-peak character reflects a double-gap feature for the SDW state in BaFe_2As_2 . Superconducting $\text{Ba}_{0.6}\text{K}_{0.4}\text{Fe}_2\text{As}_2$ also shows a weak double-gap feature (the absorption edge for the second gap is marked by arrow). Inset: optical conductivity calculated by Eq.3 (one isotropic gap) for case I and case II coherence factors at $T=0$.

(case I), σ_1^S/σ_1^N shows an asymmetry peak at the gap energy 2Δ , while for a BCS superconductor (case II) σ_1^S/σ_1^N increases gradually above 2Δ . As T/T_c (or T/T_{SDW}) appears in the exponent factor ($1/[\exp(\Delta/k_B T)+1]$) for numerical integration, deviation from the $T=0\text{ K}$ case can be neglected when $T \ll T_c$ (or $T \ll T_{SDW}$). The calculation can be further extended into the multiple-gap case, for instance, two BCS gaps on different Fermi surfaces. Model calculation for the two-gap case has been done by Barabash and Stroud.[77]

Figure 13 shows the normalized optical conductivity σ_1^S/σ_1^N in the broken symmetry state for two 122-type single crystals (the SDW state for BaFe_2As_2 parent compound and the superconducting state for $\text{Ba}_{0.6}\text{K}_{0.4}\text{Fe}_2\text{As}_2$). Different from the single-gap case as shown in the inset of Fig.13, the optical conductivity for BaFe_2As_2 has a double-peak character with two energy scales ($\Delta_1 \equiv 2\Delta^{\min}$ and $\Delta_2 \approx 2\Delta_1$). In addition, both peaks in σ_1^S/σ_1^N for BaFe_2As_2 deviate from the very sharp peak from theoretical calculation of the isotropic gap as shown in the inset figure. Even for the lowest temperature $T=10\text{ K}$, the double peaks are still rather broad and round in shape, then one can hardly fit these experimental data by two isotropic gaps with the case I coherence factor. This could be in part attributed to the very complicated band structure with only partially gapped Fermi surfaces in the SDW ordered state.

Similar to the SDW double-gap in the parent compound, the superconducting $\text{Ba}_{0.6}\text{K}_{0.4}\text{Fe}_2\text{As}_2$ also shows a double-gap character after a normalization process for the optical conductivity (the onset of the second gap is marked by the arrow). As shown below, here the symmetry of the superconducting gap is s-wave. Using a two-gap model ($\Delta_1=7\text{ meV}$ and $\Delta_2=12\text{ meV}$, we can reasonably reproduce the experimental data, while the calculation for a single gap at 7 meV shows larger discrepancy in the low frequency region (Fig.14). Then one could find that the onset of optical excitation is determined by the smaller gap, but the fine structure in $\sigma_1(\omega)$ and the characteristic energy scale in R_s/R_n are dependent on the larger gap. Since the two-component s-wave gap function can well reproduce

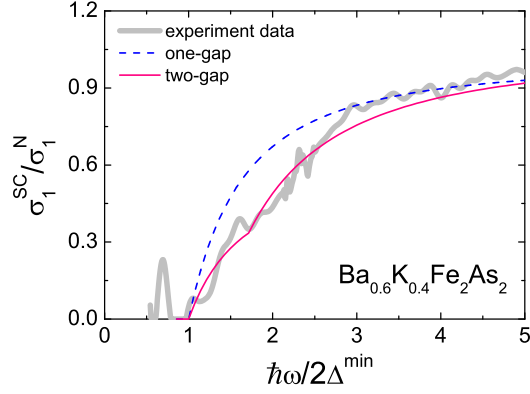


Figure 14: The optical conductivity ratio $\sigma_1^{10K}/\sigma_1^{45K}$ compared with the one-gap ($\Delta_1=7$ meV) and two-gap ($\Delta_1=7$ meV and $\Delta_2=12$ meV) fit for the BCS ground state.

the experimental character, the superconducting gaps in optimally doped (Ba,K)Fe₂As₂ should be two individual isotropic gaps on separated Fermi surfaces, which agrees well with recent ARPES observation.[73, 75] More interestingly, ARPES studies find the larger superconducting gap comes from the α and γ Fermi pockets which are well connected by the SDW vector \mathbf{q} in the parent compound, thus the inter-band interactions might play important role in the superconducting pairing, as expected also by theoretical calculations.[46] Further spectroscopic evidence for the connection between nesting vector and superconducting gap can be found in another recent ARPES study on BaFe_{1.85}Co_{0.15}As₂ (an optimally electron-doped 25.5 K superconductor), in which the α pocket disappears because of electron doping, and the superconducting gap in β pocket is then comparable with that on γ pocket (here γ is well connected with β by the vector \mathbf{q} after Co doping).[52]

4. Electronic Correlation

Investigation on Fe-based materials is believed to promote the research of finding new types of superconductors with higher T_c . On the other hand, experimental study on the similarities and differences between Fe-based superconductors and the high- T_c cuprates should help for elucidating the role of magnetic fluctuations in the superconducting pairing. Optical studies on the normal state properties for single crystalline LaFePO[78] and Ba_{0.55}K_{0.45}Fe₂As₂[70] suggest that the many-body effects cannot be neglected.

4.1. Electron-boson coupling in LaFePO

LaFePO is the first superconducting Fe-based compound discovered by Hosono's group in 2006.[79] It is also the first 1111-type compound from which relatively large single crystal has been successfully synthesized.[80] Unlike the FeAs-based compounds, LaFePO does not have the antiferromagnetic transition at high temperature. A recent study on ReFePO (Re=La, Pr, Nd) single crystals finds a different T_c evolution that T_c decreases as Ln is varied from La to Sm for ReFePO

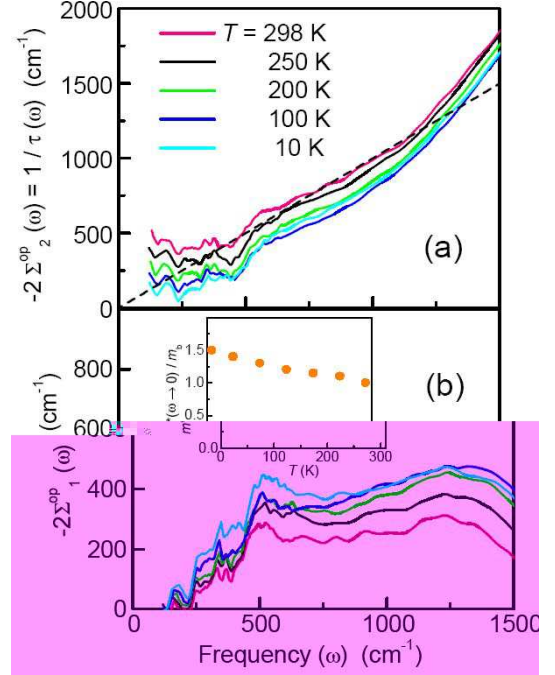


Figure 15: The frequency dependence of the (a) imaginary part of the optical quasiparticle self energy $-2\Sigma_2^{op}(\omega)$ (or scattering rate $1/\tau(\omega)$), and (b) the real part of the optical quasiparticle self energy $-2\Sigma_1^{op}(\omega)$ for LaFePO in the normal state. The dashed line in panel (a) represents the $1/\tau=\omega$ line. The inset in panel (b) shows the mass enhancement factor m^*/m_b for $\omega \rightarrow 0$. [78]

but increases for ReFeAsO_{1-x}F_x. [81] In addition, a linear T -dependence for the penetration depth is found for LaFePO, [82] suggesting a different superconducting mechanism in FeP- and FeAs-based superconductors. However, as large single crystalline 1111-type FeAs-based superconductor is still unavailable at present, spectroscopic study on LaFePO is useful to understanding the normal state properties for the Fe-based parent compound. Recent ARPES investigation indicates the ground state for LaFePO is itinerant, with no low-energy kink and no pseudogap for the bands near E_F , thus is clearly distinguishable from copper oxide superconductors. [83]

Although the ARPES study does not find any low-energy kink for LaFePO single crystal, there is an optical evidence for a 62 meV electron-boson coupling mode in the optical quasiparticle self-energy. [78] From Qazilbash *et al.*'s data, the Drude term in $\sigma_1(\omega)$ is well separated from the high energy interband transitions (see Fig. 2 in their paper [78]), thus an extended Drude analysis is used to extract the optical quasiparticle self-energy ($\Sigma_1^{op}(\omega)$, $\Sigma_2^{op}(\omega)$) from the real and imaginary parts of the optical conductivity. Then the scattering rate $1/\tau(\omega)$ and mass enhancement factor $m^*(\omega)/m_b$ can be obtained from the optical quasiparticle self-energy by

$$-2 \sum_2^{op}(\omega) = \frac{1}{\tau(\omega)} = \frac{\omega_p^2}{4\pi} \left(\frac{\sigma_1(\omega)}{\sigma_1^2(\omega) + \sigma_2^2(\omega)} \right) \quad (4)$$

$$1 - \frac{2}{\omega} \sum_1^{op}(\omega) = \frac{m^*(\omega)}{m_b} = \frac{\omega_p^2}{4\pi} \left(\frac{\sigma_2(\omega)}{\sigma_1^2(\omega) + \sigma_2^2(\omega)} \right) \quad (5)$$

As the Fe-based superconductors are multi-band systems, here the self-energy should be regarded as an average of the contributions from the relevant bands.

As shown in Fig. 15a, the scattering rate $1/\tau(\omega)$ continuously increases with frequency up to 1500 cm^{-1} with no saturation. A small kink with weak temperature dependence could be found around 500 cm^{-1} . This kink in $1/\tau(\omega)$ corresponds to the 500 cm^{-1} peak in the real part of the self-energy (Fig. 15). Qazilbash *et al.* attribute this low energy feature to an electron-boson coupling mode as found in the high- T_c cuprates.[84, 85] Figure 15a also plots the $\omega\tau=1$ line and the scattering rate $1/\tau(\omega)$ at 10 K lies below this reference line, indicating well-defined quasiparticle excitations exist in LaFePO. The overall behavior of $1/\tau(\omega)$ is different from the optimally doped cuprates, in which a linear frequency dependence is found.[84] From the inset of Fig. 15b, the mass enhancement factor ($\omega \rightarrow 0$) at $T=10 \text{ K}$ is 1.5 ± 0.1 , in good agreement with the renormalization factor of 2 obtained from ARPES and de Haas-van Alphen measurements.[83, 86] Considering the rather modest mass enhancement factor and its weak T -dependence, Qazilbash *et al.* conclude LaFePO is a moderately correlated metal.

4.2. $\text{Ba}_{0.55}\text{K}_{0.45}\text{Fe}_2\text{As}_2$

Yang *et al.* investigate the normal state properties for $\text{Ba}_{0.55}\text{K}_{0.45}\text{Fe}_2\text{As}_2$ single crystal and also find evidence for bosonic mode coupling.[70] Since it is difficult to separate the Drude component and the interband transitions in K-doped BaFe_2As_2 , several fits are used to extract the intra-band contribution for the extended Drude analysis. A bosonic excitation spectrum based on the spin fluctuation model was used to fit the scattering rate $1/\tau(\omega)$. The author find the coupling constant strongly dependent on temperature ($\lambda=0.6$ when $T=295 \text{ K}$, $\lambda=2.0$ for $T=28 \text{ K}$), suggesting that magnetic excitations are responsible for the scattering. A recent ARPES study in optimally doped $\text{Ba}_{0.6}\text{K}_{0.4}\text{Fe}_2\text{As}_2$ have found an unconventional mode with an orbital selective nature: a 25 meV mode exists for both the α and γ bands, showing a strong temperature dependence and vanishes above T_c , while no kink is found for the β band.[87] As the α and γ Fermi surfaces are well connected by the SDW vector in the parent compound, Richard *et al.* therefore speculate the kink may originate from the enhanced antiferromagnetic fluctuations below T_c .

5. Phonon

5.1. ReFeAsO system

The 1111-phase belongs to space group $P4/nmm$ and point group D_{4h} . The rare-earth ions, Fe, As and O(F) occupy 2c, 2b, 2c and 2a positions, respectively. Formal group analysis gives eight Raman active modes including two A_{1g} , two B_{1g} and four E_g modes, and six infrared active modes including three A_{2u} and three E_u modes. Representatively eight Raman active modes of LaFeAsO are shown in Fig. 16.[88] The first polarized Raman phonon measurements on La(Sm)FeAsO were made by Hadjiev *et al.* under a microscope on very small plate-like single crystals obtained within polycrystalline samples.[89]

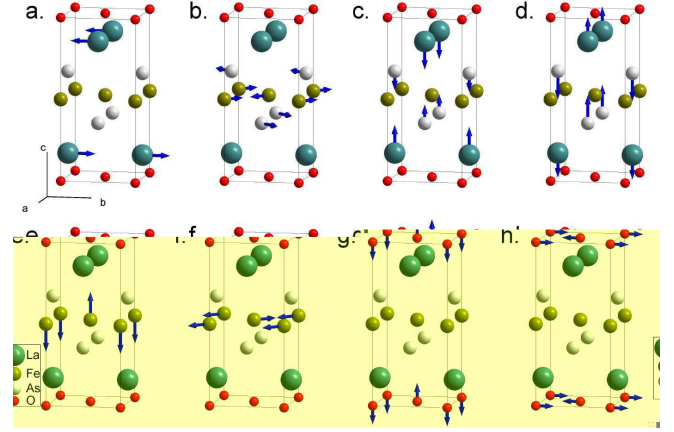


Figure 16: Eight Raman active modes of LaFeAsO in a 1111-phase representative. (a) E_g of La; (b) E_g of As and Fe; (c) A_{1g} of La; (d) A_{1g} of As; (e) B_{1g} of Fe; (f) E_g of Fe; (g) B_{1g} of O; (h) E_g of O.[88] According to the Raman tensors, doubly-degenerated E_g modes can not be determined by the ab-plane Raman measurements.

The four Raman modes with vibration out of FeAs plane were identified clearly, as shown in Fig. 17. Zhao *et al.* reported Raman spectra obtained in doped and undoped LaFeAsO(F) and CeFeAsO(F) polycrystalline samples.[88] Zhang *et al.* studied the doping and temperature dependence of Raman spectra in $\text{NdFeAsO}_{1-x}\text{F}_x$ polycrystalline samples.[90] Polarized Raman spectra on $\text{NdFeAsO}_{1-x}\text{F}_x$ single crystals were presented by Gallais *et al.*[91] Interestingly, a strong resonant enhancement for the Fe-related phonon modes was found below 2 eV , which was considered to be related to the interband transition at 2 eV as observed in optical conductivity. Among all the Raman-active phonon modes, the B_{1g} mode of iron around 210 cm^{-1} is much more important in exploring the superconducting and SDW mechanism for Fe-based compounds. However, this mode is slightly sample-dependent from the above Raman measurements.

5.2. AFe_2As_2 system

The 122-phase belongs to space group $I4/mmm$ and point group D_{4h} . Alkaline-earth ions, Fe and As occupy 2a, 4d and 4e positions, respectively. There are four Raman active modes including A_{1g} , B_{1g} and two E_g modes, and four infrared modes including two A_{2u} and two E_u modes. Litvinchuk *et al.* carried out the Raman measurements on $\text{Sr}_{1-x}\text{K}_x\text{Fe}_2\text{As}_2$ crystals (shown in Fig. 18),[92] and Choi *et al.* reported Raman results on CaFe_2As_2 crystals.[93] Compared to the 1111 phase, B_{1g} phonon frequency in the 122-phase is almost the same as that in the 1111-phase, reflecting the fact that the vibration of Fe is dominated by Fe-As bonds.

5.3. $\text{Fe}(\text{SeTe})$ system

$\text{Fe}(\text{SeTe})$ is a prototype of Fe-based superconductors, which has the simplest formula without any separation layer. Its space group is $P4/nmm$ and point group D_{4h} . Fe and Se(Te) occupy 2a and 2c positions, respectively. It has four Raman modes including A_{1g} , B_{1g} and two E_g , and two infrared modes: A_{2u}

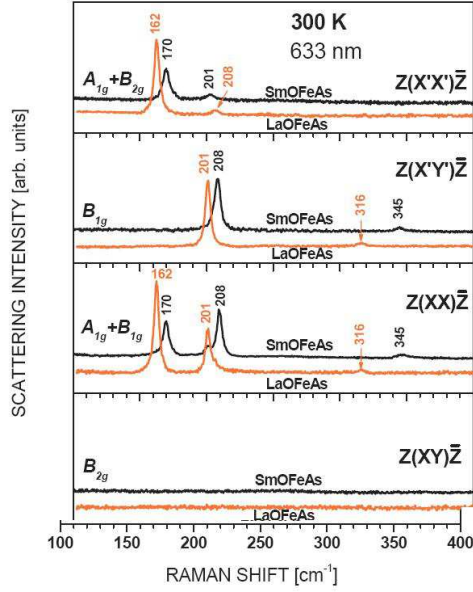


Figure 17: Polarized Raman spectra of LaFeAsO and SmFeAsO. The modes located at 208/201 cm^{-1} and 170/162 cm^{-1} corresponds to B_{1g} phonons of Fe and A_{1g} phonons of As in SmFeAsO/LaFeAsO, respectively. The 345 and 316 cm^{-1} features with weaker intensities are oxygen-related E_g modes. [89]

and E_u . As shown in Fig. 19, A_{1g} mode of Te locates at 159 cm^{-1} . B_{1g} mode of Fe is 196 cm^{-1} , slightly lower than that of FeAs-based compounds.[94] The difference can be explained as the change from Fe-As to Fe-Se(Te) bonds.

5.4. Electron-phonon coupling and isotope effect

There is no consensus on the strength of electronic correlation in the Fe-based systems yet. The role played by electron-phonon coupling is not clear for FeAs-based superconductors, although a number of theoretical calculations tend to rule out the electron-phonon coupling in the pairing.[34, 35, 46] The available Raman data do not show any evidence of strong electron-phonon coupling in terms of phonon lineshape and width.[88, 89, 91, 92, 93] However, a direct isotope experiment made by Liu *et al.*[95] indicated that the isotope effect of iron on superconducting and SDW transitions is quite large. The isotope effect is ~ 0.4 , close to conventional BCS value. While the isotope effect of oxygen on T_c is negligibly small. Apparently, further experiments are required to understand the issue. Recent X-Ray inelastic scattering experiment may present some hints on this question. It is suggested that a unconventional electron-phonon coupling may exist at certain wave vectors.[96, 97, 98]

5.5. Phonon behavior at the SDW/SC transitions

The SDW transition in the parent compounds is usually accompanied by a structural change. One may expect that phonon anomalies can be observed around the SDW transition temperatures. In principle the doubly-degenerated E_g modes of Fe will be split to B_{2g} and B_{3g} modes after the transition from tetragonal to orthorhombic structures. There is no such splitting reported yet. The estimated splitting could be too small to be

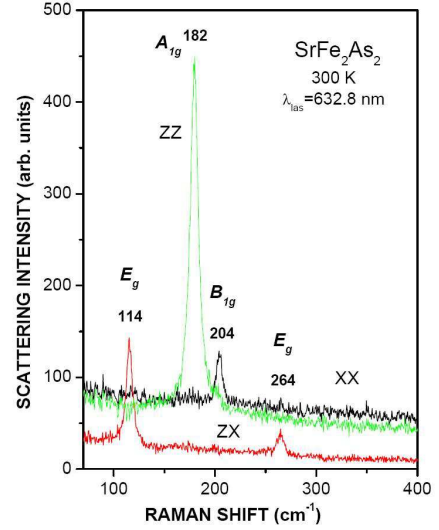


Figure 18: Polarized Raman spectra of SrFe_2As_2 crystal at room temperature. The peaks at 204 and 182 cm^{-1} are one-dimensional Fe B_{1g} and As A_{1g} modes, respectively. Doubly-degenerated E_g modes of As and Fe were detected on ac-surface. [92]

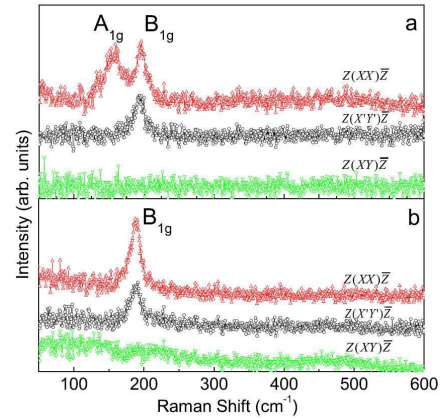


Figure 19: Polarized Raman spectra of $\text{FeTe}_{0.92}$ and $\text{Fe}_{1.03}\text{Se}_{0.3}\text{Te}_{0.7}$ crystals at room temperature. (a) Fe B_{1g} and As A_{1g} phonons can be found in the parent compounds, (b) A_{1g} phonons disappear in Se-doped FeTe.[94]

determined. However Raman measurements on SrFe_2As_2 crystals do not show such anomalies for the in-plane modes.[92] On the other hand, Raman measurements on CaFe_2As_2 crystals indicate that a large jump of $\sim 4 \text{ cm}^{-1}$ of Fe B_{1g} phonon occurs around the structural transition temperature 173 K.[93] The jump can not be explained by lattice distortion. It is suggested that the jump could be related to the change of electronic density at Fermi surface modified by structural transitions. For superconducting $\text{Sr}_{1-x}\text{K}_x\text{Fe}_2\text{As}_2$ and $\text{NdFeAsO}_{1-x}\text{F}_x$ crystals, no phonon anomalies can be seen cross T_c . [91, 92]

As shown in Fig. 2, five pronounced phonon modes at 100, 247, 265, 336, 438 cm^{-1} dominate the far-infrared reflectivity $R(\omega)$ for polycrystalline LaFeAsO.[5] According to calculated PDOS (phonon density of states), the phonon modes above 300 cm^{-1} are strongly oxygen-derived, while the phonons below 300 cm^{-1} are a mixture of La, Fe, and As vibration

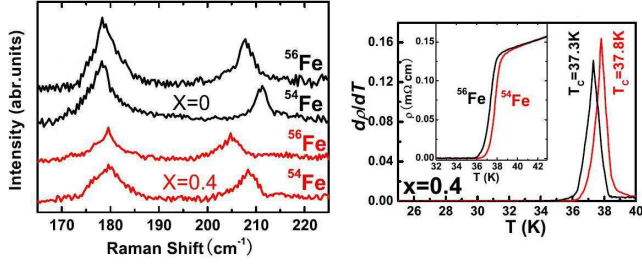


Figure 20: Left panel: Raman phonon shift of Fe isotope. An obvious shift of Fe B_{1g} mode can be resolved when replacing ^{56}Fe with ^{54}Fe isotope. Right panel: Isotope effect on T_c . [95]

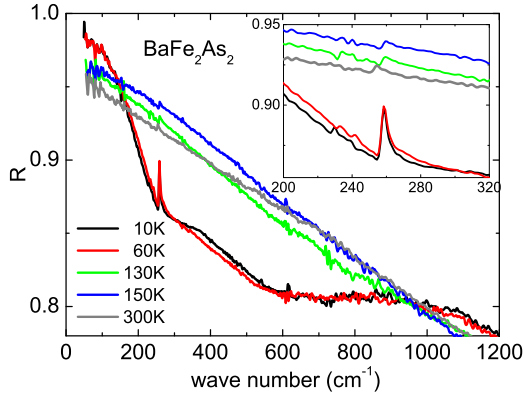


Figure 21: Reflectivity $R(\omega)$ for BaFe_2As_2 single crystal below 1200 cm^{-1} . The inset is an enlarged plot to clearly illustrate the infrared-active phonon around 259 cm^{-1} . This phonon exists for all temperatures.

modes.[34, 35] All phonon modes seems unchanged across the 150 K transition, which is later identified as a structural transition (from $P4/nmm$ to $Cmma$) by neutron scattering.[6] Yildirim calculates the IR-active phonon modes and finds such a structural distortion will not introduce new phonons at the zone center Γ , but just split the doubly degenerate modes into nondependence ones and the splitting is smaller than 0.2 meV , hence no new phonons appear in the optical reflectivity for LaFeAsO after the structural transition.[27]

Figure 21 is the ab-plane optical reflectivity for single crystalline BaFe_2As_2 . Only one infrared-active phonon mode around 259 cm^{-1} is found. Similar to the ReFeAsO case, here no new phonons appear in the spin-density wave state. As shown in the inset figure, this 259 cm^{-1} phonon exists even in 300 K, which apparently turns sharper in 10 K. This phonon can also be found in optimally doped $(\text{Ba},\text{K})\text{Fe}_2\text{As}_2$ (see Fig. 12) but is much weaker due to a better screening of itinerant carriers after K doping.

6. Conclusion

Almost one year has passed since the discovery of a 26 K superconductor $\text{LaFeAsO}_{1-x}\text{F}_x$. Besides the exploration for new types of Fe-based superconductor with higher T_c , great efforts

have been devoted to finding out how and why superconductivity emerges from Fe $3d$ electrons. In retrospect, the most convinced and important spectroscopic results were obtained from 1111-type polycrystals and 122-type single crystals for the in-plane optical response. From the SDW gap in the metallic parent compounds, and the superconducting gap for the doped systems, we know the Fe-based superconductors (especially the 122 system) are different from the high- T_c cuprates but more or less closer to the standard BCS superconductors. However, information on the charge dynamics for the c-axis, or the symmetry of the superconducting gap in single crystalline 1111-type Fe-based superconductor is still lacking. Moreover, investigations on the electronic correlation and the pseudogap-like feature in Fe-based compounds requires further studies, especially spectroscopic investigations on high-quality single crystals. Anyhow, some basic conclusions on Fe-based superconductors and their parent compounds can be made based on current optical and Raman data, which are briefly summarized as below.

Itinerant system. Almost all Fe-based superconducting systems are metallic in nature. In particular, the parent compound is not an antiferromagnetic Mott insulator, but a semimetal with an SDW instability. The plasma frequency in the normal phase (above T_{SDW}) is about 1.5 eV . When the nesting condition is weakened by either carrier doping or application of pressure, superconductivity wins in the ground state.

Multi-band effect. Fe-based superconductors are multi-band systems, which are different from the situation in cuprates (one-band). The BCS double-gap is observed in $\text{Ba}_{0.6}\text{K}_{0.4}\text{Fe}_2\text{As}_2$ from ARPES measurement. With a detailed analysis of the optical conductivity, similar two-gap superconductivity can also be found in optical response. Another optical evidence for the multi-band property in iron arsenide is the SDW double-gap in AFe_2As_2 (Sr, Ba) parent compounds.

s-wave superconductivity. From optical measurement on polycrystalline $\text{ReFeAsO}_{1-x}\text{F}_x$, signature of the superconducting gap is observed at the far-infrared as an up-turn in reflectivity below T_c . More convinced evidence of the gap symmetry comes from optical data on single crystal. For optimally doped $(\text{Ba},\text{K})\text{Fe}_2\text{As}_2$, an s-wave pairing lineshape is found for the superconducting gap, thus different from the d-wave gap in cuprates.

Electron-phonon coupling The large isotope effect implies that electron-phonon coupling may be strong in the system. However, considering its high T_c , it is unlikely that electron-phonon coupling dominates the pairing as that in conventional BCS superconductors. This issue needs further experimental and theoretical efforts in the future.

7. Acknowledgement

This work is supported by the National Science Foundation of China, the Knowledge Innovation Project of the Chinese Academy of Sciences, and the 973 project of the Ministry of Science and Technology of China.

References

- [1] Y. Kamihara, T. Watanabe, M. Hirano, and H. Hosono, *J. Am. Chem. Soc.* **130**, 3296 (2008).
- [2] X. H. Chen, T. Wu, G. Wu, R. H. Liu, H. Chen, and D. F. Fang, *Nature* **453**, 761 (2008).
- [3] G. F. Chen, Z. Li, D. Wu, G. Li, W. Z. Hu, J. Dong, P. Zheng, J. L. Luo, and N. L. Wang, *Phys. Rev. Lett.* **100**, 247002 (2008).
- [4] Z. A. Ren, W. Lu, J. Yang, W. Yi, X. L. Shen, Z. C. Li, G. C. Che, X. L. Dong, L. L. Sun, F. Zhou, and Z. X. Zhao, *Chin. Phys. Lett.* **25**, 2215 (2008)
- [5] J. Dong, H. J. Zhang, G. Xu, Z. Li, G. Li, W. Z. Hu, D. Wu, G. F. Chen, X. Dai, J. L. Luo, Z. Fang, and N. L. Wang, *Europhys. Lett.* **83**, 27006 (2008).
- [6] Clarina de la Cruz, Q. Huang, J. W. Lynn, Jiying Li, W. Ratcliff II, J. L. Zarestky, H. A. Mook, G. F. Chen, J. L. Luo, N. L. Wang, and Pengcheng Dai, *Nature* **453**, 899 (2008).
- [7] Marianne Rotter, Marcus Tegel, Dirk Johrendt, Inga Schellenberg, Wilfried Hermes, and Rainer Pöttgen, *Phys. Rev. B* **78**, 020503(R) (2008).
- [8] Marianne Rotter, Marcus Tegel, and Dirk Johrendt, *Phys. Rev. Lett.* **101**, 107006 (2008).
- [9] C. Krellner, N. Caroca-Canales, A. Jesche, H. Rosner, A. Ormeci, and C. Geibel, *Phys. Rev. B* **78**, 100504(R) (2008) .
- [10] G. F. Chen, Z. Li, G. Li, W. Z. Hu, J. Dong, P. Zheng, N. L. Wang and J. L. Luo, *Chin. Phys. Lett.* **25**, 3403 (2008).
- [11] Q. Huang, Y. Qiu, Wei Bao, J.W. Lynn, M.A. Green, Y. Chen, T. Wu, G. Wu, and X.H. Chen, *Phys. Rev. Lett.* **101**, 257003 (2008).
- [12] Jun Zhao, W. Ratcliff II, J. W. Lynn, G. F. Chen, J. L. Luo, N. L. Wang, Jiangping Hu, and Pengcheng Dai, *Phys. Rev. B* **78**, 140504(R) (2008).
- [13] N. Ni, S. L. Bud'ko, A. Kreyssig, S. Nandi, G. E. Rustan, A. I. Goldman, S. Gupta, J. D. Corbett, A. Kracher, and P. C. Canfield, *Phys. Rev. B* **78**, 014507 (2008).
- [14] G. F. Chen, Z. Li, J. Dong, G. Li, W. Z. Hu, X. D. Zhang, X. H. Song, P. Zheng, N. L. Wang, and J. L. Luo, *Phys. Rev. B* **78**, 224512 (2008).
- [15] H. S. Jeevan, Z. Hossain, Deepa Kasinathan, H. Rosner, C. Geibel, and P. Gegenwart, *Phys. Rev. B* **78**, 052502 (2008)
- [16] Zhi Ren, Zengwei Zhu, Shuai Jiang, Xiangfan Xu, Qian Tao, Cao Wang, Chunmu Feng, Guanghan Cao, and Zhu'an Xu, *Phys. Rev. B* **78**, 052501 (2008).
- [17] Fong-Chi Hsu, Jiu-Yong Luo, Kuo-Wei Yeh, Ta-Kun Chen, Tzu-Wen Huang, Phillip M. Wu, Yong-Chi Lee, Yi-Lin Huang, Yan-Yi Chu, Der-Chung Yan, and Maw-Kuen Wu, *Proc. Nat. Acad. Sci.* **105**, 14262(2008).
- [18] Kuo-Wei Yeh, Tzu-Wen Huang, Yi-Lin Huang, Ta-Kun Chen, Fong-Chi Hsu, Phillip M. Wu, Yong-Chi Lee, Yan-Yi Chu, Chi-Lian Chen, Jiu-Yong Luo, Der-Chung Yan, and Maw-Kuen Wu, *Europhys. Lett.* **84**, 37002(2008).
- [19] X.C. Wang, Q.Q. Liu, Y.X. Lv, W.B. Gao, L.X. Yang, R.C. Yu, F.Y. Li, and C.Q. Jin, *Solid State Communications*, **148**, 538 (2008).
- [20] J.H. Tapp, Z. Tang, B. Lv, K. Sasmal, B. Lorenz, C.W. Chu, and A.M. Guloy, *Phys. Rev. B* **78**, 060505(R) (2008).
- [21] Michael J. Pitcher, Dinah R. Parker, Paul Adamson, Sebastian J. C. Herkelrath, Andrew T. Boothroyd, and Simon J. Clarke, *Chemical Communications* 5918 - 5920 (2008).
- [22] M. V. Sadovskii, arXiv:0812.0302.
- [23] G. F. Chen, Z. Li, G. Li, J. Zhou, D. Wu, J. Dong, W. Z. Hu, P. Zheng, Z. J. Chen, H. Q. Yuan, J. Singleton, J. L. Luo, and N. L. Wang, *Phys. Rev. Lett.* **101**, 057007 (2008).
- [24] A. Dubroka, K.W. Kim, M. Rössle, V. K. Malik, A. J. Drew, R. H. Liu, G. Wu, X. H. Chen, and C. Bernhard, *Phys. Rev. Lett.* **101**, 097011 (2008).
- [25] W. Z. Hu, J. Dong, G. Li, Z. Li, P. Zheng, G. F. Chen, J. L. Luo, and N. L. Wang, *Phys. Rev. Lett.* **101**, 257005(2008).
- [26] G. Li, W. Z. Hu, J. Dong, Z. Li, P. Zheng, G. F. Chen, J. L. Luo, and N. L. Wang, *Phys. Rev. Lett.* **101**, 107004 (2008).
- [27] T. Yildirim, *Phys. Rev. Lett.* **101**, 057010 (2008).
- [28] Fengjie Ma, Zhong-Yi Lu, and Tao Xiang, *Phys. Rev. B* **78**, 224517 (2008).
- [29] Chen Fang, Hong Yao, Wei-Feng Tsai, JiangPing Hu, and Steven A. Kivelson, *Phys. Rev. B* **77**, 224509 (2008).
- [30] Cenke Xu, Markus Mueller, and Subir Sachdev, *Phys. Rev. B* **78**, 020501(R) (2008).
- [31] C. Marini, C. Mirri, G. Profeta, S. Lupi, D. Di Castro, R. Socracase, P. Postorino, P. Calvani, A. Perucchi, S. Massidda, G. M. Tropeano, M. Putti, A. Martinelli, A. Palenzona, and P. Dore, arXiv:0810.2176.
- [32] M. Tropeano, C. Fanciulli, C. Ferdeghini, D. Marrè, A.S. Siri, M. Putti, A. Martinelli, M. Ferretti, A. Palenzona, M. R. Cimberle, C. Mirri, S. Lupi, R. Socracase, P. Calvani, and A. Perucchi, arXiv:0809.3500.
- [33] J. Zhao, Q. Huang, C. de la Cruz, S. Li, J. W. Lynn, Y. Chen, M. A. Green, G. F. Chen, G. Li, Z. Li, J. L. Luo, N. L. Wang, and Pengcheng Dai, *Nature Materials* **7**, 953 (2008).
- [34] D. J. Singh and M.-H. Du, *Phys. Rev. Lett.* **100**, 237003(2008).
- [35] L. Boeri, O. V. Dolgov, and A. A. Golubov, *Phys. Rev. Lett.* **101**, 026403(2008).
- [36] A. V. Boris, N. N. Kovaleva, S. S. A. Seo, J. S. Kim, P. Popovich, Y. Matiks, R. K. Kremer, and B. Keimer, *Phys. Rev. Lett.* **102**, 027001 (2009).
- [37] W. Z. Hu, et al. unpublished data.
- [38] D. J. Singh, *Phys. Rev. B* **78**, 094511 (2008).
- [39] L. X. Yang, Y. Zhang, H. W. Ou, J. F. Zhao, D. W. Shen, B. Zhou, J. Wei, F. Chen, M. Xu, C. He, Y. Chen, Z. D. Wang, X. F. Wang, T. Wu, G. Wu, X. H. Chen, M. Arita, K. Shimada, M. Taniguchi, Z. Y. Lu, T. Xiang, and D. L. Feng, arXiv:0806.2627.
- [40] C. Liu, G. D. Samolyuk, Y. Lee, N. Ni, T. Kondo, A. F. Santander-Syro, S. L. Bud'ko, J. L. McChesney, E. Rotenberg, T. Valla, A. V. Fedorov, P. C. Canfield, B. N. Harmon, and A. Kaminski, *Phys. Rev. Lett.* **101**, 177005 (2008).
- [41] D. Hsieh, Y. Xia, L. Wray, D. Qian, K.K. Gomes, A. Yazdani, G.F. Chen, J.L. Luo, N.L. Wang, and M.Z. Hasan, arXiv:0812.2289.
- [42] M. Dressel, and G. Grüner, *Electrodynamics of Solids*, Cambridge University Press (2002).
- [43] Suchitra E. Sebastian, J. Gillett, N. Harrison, C. H. Mielke, S. K. Goh, P. H. C. Lau, and G. G. Lonzarich, *J. Phys.: Condens. Matter* **20**, 422203 (2008).
- [44] Q. Si, and E. Abrahams, *Phys. Rev. Lett.* **101**, 076401 (2008).
- [45] J. Wu, P. Phillips, and A. H. Castro Neto, *Phys. Rev. Lett.* **101**, 126401 (2008).
- [46] I. I. Mazin, D. J. Singh, M. D. Johannes, and M. H. Du, *Phys. Rev. Lett.* **101**, 057003 (2008).
- [47] Vladimir Cvetkovic and Zlatko Tesanovic, arXiv:0804.4678.
- [48] Haiyun Liu, Wentao Zhang, Lin Zhao, Xiaowen Jia, Jianqiao Meng, Guodong Liu, Xiaoli Dong, G. F. Chen, J. L. Luo, N. L. Wang, Wei Lu, Guiling Wang, Yong Zhou, Yong Zhu, Xiaoyang Wang, Zuyan Xu, Chuangtian Chen, and X. J. Zhou, *Phys. Rev. B* **78**, 184514 (2008)
- [49] H. Ding, K. Nakayama, P. Richard, S. Souma, T. Sato, T. Takahashi, M. Neupane, Y.-M. Xu, Z.-H. Pan, A.V. Federov, Z. Wang, X. Dai, Z. Fang, G.F. Chen, J.L. Luo, and N.L. Wang, arXiv:0812.0534.
- [50] T. Sato, K. Nakayama, Y. Sekiba, P. Richard, Y.-M. Xu, S. Souma, T. Takahashi, G. F. Chen, J. L. Luo, N. L. Wang, and H. Ding, arXiv:0810.3047.
- [51] Y. Sekiba, T. Sato, K. Nakayama, K. Terashima, P. Richard, J. H. Bowen, H. Ding, Y.-M. Xu, L. J. Li, G. H. Cao, Z.-A. Xu, and T. Takahashi, arXiv:0812.4111.
- [52] K. Terashima, Y. Sekiba, J. H. Bowen, K. Nakayama, T. Kawahara, T. Sato, P. Richard, Y.-M. Xu, L. J. Li, G. H. Cao, Z.-A. Xu, H. Ding, and T. Takahashi, arXiv:0812.3704.
- [53] W. Bao, Y. Qiu, Q. Huang, A. Green, P. Zajdel, M.R. Fitzsimmons, M. Zhernenkov, M. Fang, B. Qian, E.K. Vehstedt, J. Yang, H.M. Pham, L. Spinu, and Z.Q. Mao, arXiv:0809.2058.
- [54] Shiliang Li, Clarina de la Cruz, Q. Huang, Y. Chen, J. W. Lynn, Jiangping Hu, Yi-Lin Huang, Fong-chi Hsu, Kuo-Wei Yeh, Maw-Kuen Wu, and Pengcheng Dai, arXiv:0811.0195.
- [55] F.C. Hsu, T.Y. Luo, K.W. Yeh, T.K. Chen, T.W. Huang, Phillip M. Wu, Y.C. Lee, Y.L. Huang, Y.Y. Chu, D.C. Yan, and M.K. Wu, *Proc. Natl. Acad. Sci. USA.* **105**, 14262 (2008).
- [56] M.H. Fang, H.M. Pham, B. Qian, T.J. Liu, E.K. Vehstedt, Y. Liu, L. Spinu, and Z.Q. Mao, *Phys. Rev. B* **78**, 224503 (2008).
- [57] K.W. Yeh, T.W. Huang, Y.L. Huang, T.K. Chen, F.C. Hsu, Phillip M. Wu, Y.C. Lee, Y.Y. Chu, C.L. Chen, J.Y. Luo, D.C. Yan, and M.K. Wu, arXiv:0808.0474
- [58] Y. Mizuguchi, F. Tomioka, S. Tsuda, T. Yamaguchi, and Y. Takano, *Appl. Phys. Lett.* **93**, 152505 (2008).
- [59] G. F. Chen, Z. G. Chen, J. Dong, W. Z. Hu, G. Li, X. D. Zhang, P. Zheng, J. L. Luo, and N. L. Wang, arXiv:0811.1489.

- [60] Y. Xia, D. Qian, L. Wray, D. Hsieh, G.F. Chen, J.L. Luo, N.L. Wang, and M.Z. Hasan, arXiv:0901.1299.
- [61] Lijun Zhang, D.J. Singh, and Mao-Hua Du, arXiv:0810.3274.
- [62] S.I. Mirzaei, V. Guritanu, A. B. Kuzmenko, C. Senatore, D. van der Marel, G. Wu, R. H. Liu, and X. H. Chen, arXiv:0806.2303.
- [63] S.-L. Drechsler, M. Grobosch, K. Koepfner, G. Behr, A. Köhler, J. Werner, A. Kondrat, N. Leps, Ch. Hess, R. Klingeler, R. Schuster, B. Büchner, and M. Knupfer, Phys. Rev. Lett. **101**, 257004(2008).
- [64] M. Tinkham, *Introduction to Superconductivity*(2nd Ed.), (McGraw-Hill, New York, 1996).
- [65] C. C. Homes, S. V. Dordevic, T. Valla, and M. Strongin, Phys. Rev. B **72**, 134517 (2005).
- [66] C. C. Homes, S. V. Dordevic, D. A. Bonn, Ruixing Liang, and W. N. Hardy, Phys. Rev. B **69**, 024514 (2004).
- [67] R. A. Ferrell and R. E. Glover, III, Phys. Rev. **109**, 1398 (1958).
- [68] M. Tinkham and R. A. Ferrell, Phys. Rev. Lett. **2**, 331 (1959).
- [69] C. C. Homes, R. P. S. M. Lobo, P. Fournier, A. Zimmers, and R. L. Greene, Phys. Rev. B **74**, 214515 (2006).
- [70] J. Yang, D. Hüvonen, U. Nagel, T. Rööm, N. Ni, P. C. Canfield, S. L. Bud'ko, J.P. Carbotte, and T. Timusk, arXiv:0807.1040.
- [71] H. J. A. Molegraaf, C. Presura, D. van der Marel, P. H. Kes, and M. Li, Science **295**, 2239 (2002).
- [72] F. Santander-Syro, R. P. S. M. Lobo, N. Bontemps, Z. Konstantinovic, Z. Z. Li, and H. Raffy, Europhys. Lett. **62**, 568 (2003).
- [73] H. Ding, P. Richard, K. Nakayama, T. Sugawara, T. Arakane, Y. Sekiba, A. Takayama, S. Souma, T. Sato, T. Takahashi, Z. Wang, X. Dai, Z. Fang, G. F. Chen, J. L. Luo, and N. L. Wang, Europhys. Lett. **83**, 47001 (2008).
- [74] Lin Zhao, Haiyun Liu, Wentao Zhang, Jianqiao Meng, Xiaowen Jia, Guodong Liu, Xiaoli Dong, G. F. Chen, J. L. Luo, N. L. Wang, Guiling Wang, Yong Zhou, Yong Zhu, Xiaoyang Wang, Zhongxian Zhao, Zuyan Xu, Chuangtian Chen, and X. J. Zhou, Chin. Phys. Lett. **25**, 4402(2008)
- [75] K. Nakayama, T. Sato, P. Richard, Y.-M. Xu, Y. Sekiba, S. Souma, G. F. Chen, J. L. Luo, N. L. Wang, H. Ding, and T. Takahashi, arXiv:0812.0663.
- [76] G. Grüner, *Density Waves in Solids* (Addison-Wesley, Reading, MA, 1994).
- [77] Sergey V. Barabash, and David Stroud, Phys. Rev. B **66**, 172501 (2002).
- [78] M. M. Qazilbash, J. J. Hamlin, R. E. Baumbach, M. B. Maple, and D. N. Basov, arXiv:0808.3748.
- [79] Y. Kamihara, H. Hiramatsu, M. Hirano, R. Kawamura, H. Yanagi, T. Kamiya, and H. Hosono, J. Am. Chem. Soc. **128**, 10012 (2006).
- [80] J. J. Hamlin, R. E. Baumbach, D. A. Zocco, T. A. Sayles, and M. B. Maple, J. Phys.: Condens. Matter **20**, 365220 (2008).
- [81] R. E. Baumbach, J. J. Hamlin, L. Shu, D. A. Zocco, N. M. Crisosto, and M. B. Maple, arXiv:0812.0774.
- [82] J.D. Fletcher, A. Serafin, L. Malone, J. Analytis, J-H Chu, A.S. Erickson, I.R. Fisher, and A. Carrington, arXiv:0812.3858.
- [83] D. H. Lu, M. Yi, S.-K. Mo, A. S. Erickson, J. Analytis, J.-H. Chu, D. J. Singh, Z. Hussain, T. H. Geballe, I. R. Fisher, and Z.-X. Shen, Nature **455**, 81(2008).
- [84] D. N. Basov and T. Timusk, Rev. Mod. Phys. **77**, 721 (2005).
- [85] J. Hwang, T. Timusk, and G. D. Gu, Nature **427**, 714 (2004).
- [86] A.I. Coldea, J.D. Fletcher, A. Carrington, J.G. Analytis, A.F. Bangura, J.-H. Chu, A. S. Erickson, I.R. Fisher, N.E. Hussey, and R.D. McDonald, arXiv:0807.4890.
- [87] P. Richard, T. Sato, K. Nakayama, S. Souma, T. Takahashi, Y.-M. Xu, G. F. Chen, J. L. Luo, N. L. Wang, and H. Ding, Phys. Rev. Lett. **102**, 047003 (2009).
- [88] S. C. Zhao, D. Hou, Y. Wu, T. L. Xia, A. M. Zhang, G. F. Chen, J. L. Luo, N. L. Wang, J. H. Wei, Z. Y. Lu, and Q. M. Zhang, Supercond. Sci. Technol. **22**, 015017(2009).
- [89] V. G. Hadjiev, M. N. Iliev, K. Sasmal, Y. -Y. Sun, and C. W. Chu, Phys. Rev. B **77**, 220505 (2008).
- [90] L. Zhang, T. Fujita, F. Chen, D. L. Feng, S. Maekawa, and M. W. Chen, arXiv:0809.1474.
- [91] Y. Gallais, A. Sacuto, M. Cazayous, P. Cheng, L. Fang, and H. H. Wen, Phys. Rev. B **78** (2008) 132509.
- [92] A. P. Litvinchuk, V. G. Hadjiev, M. N. Iliev, Bing Lv, A. M. Guloy, and C. W. Chu, Phys. Rev. B **78**, 060503(2008).
- [93] K.-Y. Choi, D. Wulferding, P. Lemmens, N. Ni, S. L. Bud'ko and P. C. Canfield, arXiv:0810.2040.
- [94] Tian-Long Xia, D. Hou, S. C. Zhao, A. M. Zhang, G. F. Chen, J. L. Luo, N. L. Wang, J. H. Wei, Z. -Y. Lu, and Q. M. Zhang, arXiv:0811.2350.
- [95] Tatsuo Fukuda, Alfred Q. R. Baron, Shin-ichi Shamoto, Motoyuki Ishikado, Hiroki Nakamura, Masahiko Machida, Hiroshi Uchiyama, Satoshi Tsutsui, Akira Iyo, Hijiri Kito, Jun'ichiro Mizuki, Masatoshi Arai, Hiroshi Eisaki, and Hideo Hosono, J. Phys. Soc. Jpn. **77** 103715 (2008).
- [96] M. Le Tacon, M. Krisch, A. Bosak, J.-W. G. Bos, and S. Margadonna, Phys. Rev. B **78**, 140505(R) (2008).
- [97] D. Reznik, K. Lokshin, D. C. Mitchell, D. Parshall, W. Dmowski, D. Lamago, R. Heid, K.-P. Bohnen, A. S. Sefat, M. A. McGuire, B. C. Sales, D. G. Mandrus, A. Asubedi, D. J. Singh, A. Alatas, M. H. Upton, A. H. Said, Yu. Shvyd'ko, and T. Egami, arXiv: 0810.4941.
- [98] R. H. Liu, T. Wu, G. Wu, H. Chen, X. F. Wang, Y. L. Xie, J. J. Yin, Y. J. Yan, Q. J. Li, B. C. Shi, W. S. Chu, Z. Y. Wu, and X. H. Chen, arXiv:0810.2694.